Heliyon 10 (2024) e26675

Contents lists available at ScienceDirect

Heliyon

journal homepage: www.cell.com/heliyon

Research article

Bone marrow stem cells with or without superparamagnetic iron oxide nanoparticles as a magnetic targeting tool: Which is better in regeneration of neurolysed facial nerve? An experimental study

Noura Abd El-Latif, Lecturer [a,*], Rehab R. El Zehary, Professor [b], Fatma M. Ibrahim, Professor [b], Mona Denewar, Associate Professor [c]

[a] Oral Biology, Faculty of Dentistry, Mansoura University, Egypt
[b] Oral Biology, Faculty of Dentistry, Mansoura University, Egypt
[c] Oral Biology, Faculty of Dentistry, Mansoura University, Egypt

ARTICLE INFO

Keywords:
Bone marrow stem cell
Facial nerve
Neurolysis
Magnetic targeting
Superparamagnetic iron oxide nanoparticle

ABSTRACT

Aim: This study was performed to evaluate neural regenerative capacities of bone marrow stem cells (BMSCs) with or without superparamagnetic iron oxide nanoparticles (SPIONs) as a magnetic targeting tool after neurolysis of the facial nerve (FN) in albino rats.
Methods: Thirty-eight male albino rats were selected. Two of them were euthanized for normal FN histology assessment. Thirty-six rats were injected with ethanol in the FN nerve for neurolysis induction and assessed one week post-operatively by eye blinking test. Animals were divided into three groups, each containing twelve rats: Group I (positive control) was injected with Dulbecco Modified Eagle's medium (DMEM-F12), group II was injected with BMSCs in DMEM-F12, and group III was injected with BMSCs in DMEM-F12 with poly L-lysine coated SPIONs (0.5 mmol/mL). Monitoring of SPIONs in the rat's body was carried out by MRI. A circular neodymium magnet N52 (0.57 T, 2 × 5 mm) was placed on each rat in group III just below the right ear at the site of surgery to attract SPIONs labeled BMSCs, left in place for 24 h, and then removed. From each group, six rats were euthanized at the end of the 4th and 8th week of treatment, respectively. The right FN trunks were extracted for routine histological examination using H&E stain. Immunohistochemical examination by anti-S100B was performed to characterize the thickness of the myelin sheath formed by the Schwann cells. Ultra-structural examination was performed to study changes in axons, myelin sheaths, and Schwann cells.
Results: Regeneration of nerve fibers, Schwan cells, and myelin sheaths was better in group II than in groups I and III histologically, immunohistochemically, and ultra-structurally.
Conclusion: BMSCs alone could ameliorate FN regeneration better than magnetic targeting treatment using BMSCs labeled with SPIONs.

1. Introduction

Normal facial nerve activity is very important for any person to formulate a normal physical, emotional and psychological makeup. Many vocational and social difficulties can take place if there as an impairment in the facial activity leading to facial disfigurement.

* Corresponding author.
E-mail addresses: nhm_1989@hotmail.com, nourahasan@mans.edu.eg (N.A. El-Latif).

https://doi.org/10.1016/j.heliyon.2024.e26675
Received 23 July 2023; Received in revised form 29 January 2024; Accepted 16 February 2024
Available online 17 February 2024

Facial palsy is a condition in which the facial muscles are paralyzed. If the condition is unilateral, it is known as Bell's palsy. This condition may be caused by auto-immune, metabolic or systemic diseases such as diabetes mellitus, hypertension, amyloidosis, alcoholism and toxicity. It may also take place due to local causes as neoplastic lesions, facial nerve injury, infections, or unidentified causes [1].

Neurolysis is the process of administering physically or chemically damaging agents to a nerve to establish a prolonged or persistent disruption of neural transmission. Neurolysis is appointed mainly for the treatment of intractable cancer pain. Infrequently, some types of nonmalignant pain can be managed with these neurolytic agents (for example, intractable postherpetic neuralgia and chronic pancreatitis).

Neurolysis can be induced by cooling (cryotherapy) and heating (radiofrequency lesions or laser), which are physical agents. Chemical agents commonly used are glycerol, chlorocresol, ammonium compounds, phenol, aminoglycosides, hypertonic or hypotonic solutions, and alcohols [2].

Ethanol, used in neurolysis, results in axon necrosis by coagulating protein without disrupting the Schwann cell. Cell bodies are destructed along with axons. Therefore, normal regeneration is not possible, and permanent blockade results [3].

Mesenchymal stem cells (MSCs) are kind of adult stem cells with multipotent capabilities and various benefits serving as a novel therapeutic alternative. Minor morbidity of donor-site is one of these benefits when compared to autografts, in addition to exceeding the ability of damaged tissue regeneration without fibrous tissue formation, and decreased probability of autoimmune rejection or infection [4,5].

Mesenchymal stem cells may be more beneficial in the management of various neurologic diseases in comparison with other types of stem cells. The bone marrow cells are readily accessible, overwhelming the risks of extracting neural stem cells from the central nervous system and granting a renewable population. Only a simple protocol can be used to for bone marrow stem cells (BMSCs) to be cultured and differentiated into neurons [6–8].

Many of the ongoing cell therapies, whether in-vitro or in-vivo, use systemic or local distribution of stem cells. These therapies rely on stem cell emigration and nesting at insult regions. Nonetheless, the major confrontations that face these techniques are how to determine the fate and localization of these cells, and how to retain the cells at the target site inside the body [9].

Magnetic targeting systems using magnetically labeled cells have proved to be a more efficient technique for delivering cells to target sites. These systems are based on loading stem cells with magnetic nanoparticles, followed by attracting them to particular regions inside the body by utilizing an external magnetic field [10].

Superparamagnetic iron oxide nanoparticles (SPIONs) are nowadays considered a favorable choice in nanobiotechnology for various applications. Even the biocompatibility of iron oxide compounds was under concern because the accumulation of an over-supply of ferric or ferrous ions in the cytoplasm in a non-complexed pattern can initiate biomolecular oxidation reactions [11]. Nonetheless, SPIONs showed biocompatibility with minimal toxic effects due to their surface chemical modifications using coating materials [12]. Thus, SPIONs are used nowadays in many fields, such as magnetic separation, magnetic resonance imaging (MRI) [13], magnetic hyperthermia, and drug delivery. Significantly, the site-specific drug, diagnostic agent, and stem cell delivery using SPIONs are the most exciting applications [14,15].

In this context, the investigators hypothesized that BMSCs alone or with SPIONs might have greater regenerative capacity on the neurolysed facial nerve in albino rats. The null hypothesis was considered that there was no difference in the impact of BMSCs with or without SPIONs on the regeneration of neurolysed facial nerves in albino rats.

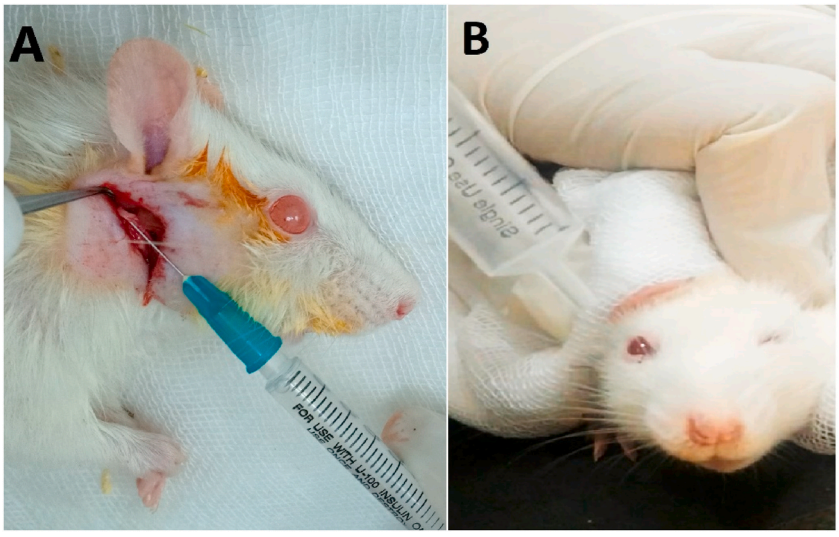

Fig. 1. Photographs showing injecting 0.01 mL of 90% alcohol within the rat's right facial nerve trunk (A). Eye blinking test after 1 week of operation with loss of blinking action in the right eye. (B).

2. Materials and methods

Thirty-eight pathogen-free male albino rats weighing 200–300 g were selected. All experimental procedures were done in accordance with the protocol accredited by the Ethical Committee of the Faculty of Dentistry, Mansoura University, Egypt (Code No. M02260219), and the Nile Center for Experimental Research Animal House Unit, Mansoura City, Egypt. The rats were provided with a standard pelleted diet and water ad libitum. They were kept in a 12-h light/dark cycle.

2.1. Study design

Two normal rats were euthanized without any intervention as a reference for normal facial nerve histology and other histological processing. Thirty-six rats received an intra-fascicular injection of 0.01 mL of 90% ethanol in the right facial nerve trunks [16] (Fig. 1A). Assessment of facial movements was carried out one week post-operatively by observation of eye blinking with air afflation. Then, animals were divided into three groups, each containing 12 rats. In Group I, animals received an intravenous injection of DMEM-F12 (0.2 mL) and were considered positive control. In Group II, animals received an intravenous infusion of 10^6 bone marrow stem cells in fresh DMEM-F12 (0.2 mL). In Group III, animals received an intravenous injection of 10^6 bone marrow stem cells in fresh DMEM-F12 (0.2 mL) with SPIO nanoparticles. Six animals from each group were euthanized at the end of the 4th week after treatment, while the remaining animals were euthanized at the end of 8th week.

2.2. Eye blinking test

A syringe of 10 cm^3 without a needle was filled with air. The rat was placed in a black cardboard box to better observe the eye blinking reflex. The rat was secured in place using a surgical pad. The syringe tip was held about 5 mm away from the right eye. Air was pressed against the eye, and the eyelids reflex was observed. The same steps were repeated for the left eye in each rat for comparison. Complete nerve degeneration was considered with total loss of blinking reflex in the right eye [17] (Fig. 1B).

2.3. Isolation and culture of BMSCs

All in vitro steps were performed in the Nile Center for Experimental Research Stem Cell Unit, Mansoura City, Egypt. Four pathogen-free albino rats weighing 80–150 g were euthanized and bone marrow tissue samples were separated. The samples were treated aseptically. Then, bone marrow samples were cultured in Dulbecco's Modified Eagle's medium Ham's F-12 (DMEM-F12) with 10% fetal bovine serum (FBS) and 1% streptomycin, penicillin, and amphotericin. Stem cell explants were incubated at 37 0C and 5% CO2 humidified air. Confluence of cell cultures was about 80% on days 14–21. Then, trypsinization of cells was performed followed by subculturing [18].

2.4. Immunophenotype determination using flow cytometry

Bone marrow cells (with total count of 5×10^5) were incubated with individual primary monoclonal antibodies. Then, their specific antigen was conjugated with fluorescein isothiocyanate (FITC) in 100 μl PBS for 20 min in the dark at room temperature. CD105,

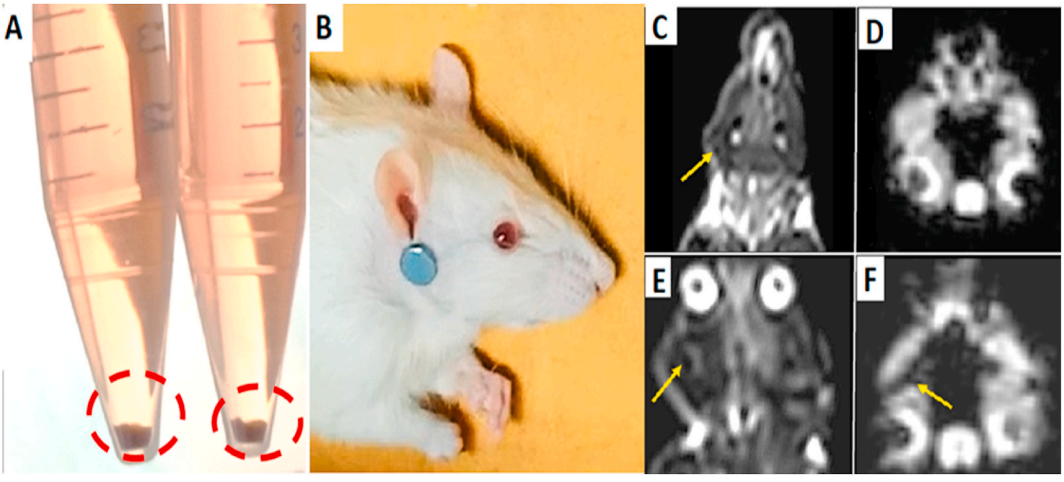

Fig. 2. Photographs showing BMSCs pellet with dark brown color indicating conjugation with SPIONs (**A**). Neodymium magnet N52 (0.57 T, 2 × 5 mm) was placed just below the rat's right ear (B). (C), (E) MRI coronal T2 weighted image. (D), (F) MRI cheek axial susceptibility weighted image. The dark areas showed by the arrows revealed appearance of MR signs of SPIONs accumulation foci at the right side of the face. (For interpretation of the references to color in this figure legend, the reader is referred to the Web version of this article.)

CD90, CD34, and CD45 were used as primary antibodies. Dilution of cells was performed in 2 mL PBS/bovine serum albumin. Then, cells were centrifuged, and resuspended in 200 μl of 4% paraformaldehyde. BD Accuri C6 flow cytometer and BD Accuri C6 software program were used for data collection and analysis.

2.5. Systemic administration of BMSCs

Plastic syringes of 100 IU were loaded with BMSCs suspension. Each syringe was loaded with 0.2 mL of complete DMEM-F12 carrying 1×10^6 BMSCs and injected through the tail vein.

2.6. BMSCs labeling with SPIONs

A sample of 25 μg Fe/mL SPIO (0.5 mmol/mL; Sigma Aldrich) was added to BMSCs. Poly-L-lysine (Cat N°: P4832 -50 ML, Sigma-Aldrich) was used as a coating material for SPIONs with a concentration of 375 ng/mL and added to the complete culture medium. The cells were cultured for 24 h at 37◦C in a 5%CO2 incubator; then the medium was discarded. The BMSCs were subsequently washed three times with PBS to remove the unlabeled SPIONs. BMSCs pellet appeared with dark brown color indicating conjugation with SPIONs. (Fig. 2A). Following trypsinization, the BMSCs were suspended in a culture medium as an injection solution for transplantation [10]. A circular neodymium magnet N52 (0.57 T, 2 × 5 mm) was placed on each rat's hair just below the right ear at the site of surgery (Fig. 2B). The magnet was fixed by a piece of surgical tape, left in place for 24 h, and then removed.

2.7. Magnetic resonance imaging after transplantation of BMSCs labeled with SPIO nanoparticles

MR imaging of the right facial nerve was performed after magnets removal using a 1.5 T clinical MR imager with a circular surface coil (diameter 11 cm). Axial images were captured using a standard T2 (transverse sequence)-weighted turbo spin-echo sequence, one of the basic sequences in MRI. The imaging sequence parameters were as follows: field of view (FOV), 80×80 mm^2; slice thickness, 2 mm; spacing, 0.5 mm; base resolution matrix, 256 × 256; repetition time (TR), 2000 ms; and effective echo time (TE), 70 ms. MRI was performed to ensure that the neodymium magnet had successfully attracted SPIONs-labeled BMSCs to the injured facial nerve.

2.8. Histological evaluation

2.8.1. Preparation of histological and immunohistochemical sections

Specimens were fixed in 10% neutral buffered formalin for 24 h. Slides were stained with hematoxylin and eosin (H & E) for routine histological examination. In addition, myelin sheath marker (anti-S100B) was applied as an immunohistochemical stain to characterize the thickness of the myelin sheath formed by the Schwann cell. S100B activates the Ras-MEK-ERK1/2-NF-κB pathway in neural cells and leads to the activation of small GTPases, Rac1/Cdc 42, and neurite growth.

2.8.2. Immunostaining evaluation

Photomicrographs of slides were obtained using a ToupView® digital camera installed on an Olympus® microscope with a 1/2 photo adaptor, using X objective. Fiji ImageJ processing package software (https://fiji.sc/) was used to analyze 20 images (10 cm width x 5 cm length) with a resolution of 300 dpi for each group. The amount of anti-S100B immunoreactivity in myelin sheaths around nerve fibers was analyzed using the threshold tool. The thresholding tool judged the percentage of immunoreactive area to each section's selected overall immunostained area.

2.8.3. Ultrastructural evaluation

Specimens were fixed immediately and primarily in glutaraldehyde 4% for 2 h, then fixed in osmic acid solution (1%) for one to 2 h. Sections were stained with 1–2 g uranyl acetate and 100 mL water, then stained in prepared lead citrate (0.4 lead citrate NaOH). Finally, they were dehydrated before examination under the transmission electron microscope (JEM-2100, JEOL, Japan).

2.8.4. Statistical analysis

Data of immunohistochemical findings were analyzed using IBM SPSS software package version 20.0. (Armonk, NY: IBM Corp). Descriptive statistics were calculated in the form of mean and standard deviation (±SD). The data were tested by two-way (ANOVA) to detect interaction between groups and time on different parameters. A probability (P) value < 0.05 was considered statistically significant.

3. Results

3.1. Cultured BMSCs morphology

BMSCs appeared as non-adherent, spherical cells on day 1 of isolation (Fig. 3A). On day 3 at the initial culture, few fibroblast-like cells adhered to the flask (Fig. 3B). On day 12, the confluence of adherent cells was about 80% (Fig. 3C). After the addition of SPIO nanoparticles, diffusion of nanoparticles inside stem cells was evident after culturing and incubation at 37◦C in a 5%CO2 for 24 h (Fig. 5A and B).

3.2. Flow cytometry characterization

The immunophenotype characterization was performed at the 3rd passage of culturing. In the cultivated specimen, positive immunostaining was detected for BMSCs, including CD105 (Fig. 4A) and CD90 (Fig. 4B), while negative or weakly positive immunostaining was detected for CD34 (Fig. 4C) and CD45 (Fig. 4D) hematopoietic markers.

3.3. MRI results after transplantation of BMSCs labeled with SPIONs

The signal intensities of the injured right facial nerve trunks in the SPIONs-labeled BMSCs groups were low after transplantation. SPIONs distorted the local magnetic field and appeared as dark foci (Fig. 2C, D, E, F).

3.4. Histological results

3.4.1. Routine histological sections

Histological results of the negative control group showed normal architecture and organization of nerve fibers and Schwann cells, with typical thickness of myelin sheaths around nerve fibers (Fig. 6A). In group I, after four weeks of treatment, the facial nerve trunks showed extensive Wallerian degeneration in the form of numerous and large areas of edema and digestion chambers containing remnants of degenerated axons (Fig. 6B).

After eight weeks in the same group, the facial nerve trunks showed fewer small digestion chambers. Increased cellularity of proliferating Schwann cells, with elongated nuclei as a response to nerve injury, was evident. Axons and Schwann cells had abnormal arrangement (Fig. 6C).

The facial nerve trunks in group II showed a tendency towards regeneration after four weeks. They revealed the presence of a minimal number of digestion chambers containing remnants of degenerated axons. Increased cellularity by proliferating Schwan cells was evident (Fig. 6D). However, after eight weeks of treatment in the same group, there was a decrease in the number and size of edematous areas and the number of digestion chambers. Axons and Schwann cells seemed to have better organization and architecture (Fig. 6E).

The facial nerve trunks of group III, after four weeks of treatment, showed attempts towards regeneration. They showed the presence of a minimal number of digestion chambers, very few remnants of degenerated axons, and proliferating Schwann cells. Axons and Schwann cells were nearly well-organized (Fig. 6F). Few signs of regeneration were observed after eight weeks in the same group. Axons and Schwann cells were not well-organized. There was a slight increase in the number and size of edematous areas and digestion chambers (Fig. 6G).

3.4.2. Immunohistochemical findings

Anti-S100B-immunostained sections of the negative control group showed mild immunoreactivity in myelin sheaths around nerve fibers (16.93 ± 0.06%) (Fig. 7A). After four weeks of treatment, group I showed mild immunoreactivity (18.21 ± 10.17%) (Fig. 7B), similar to the immunoreactivity of group I after eight weeks of treatment (13.51 ± 8.05%) (Fig. 7C). After four weeks of treatment, group II showed moderate immunoreactivity (21.99 ± 4.05%) (Fig. 7D), which increased to severe after the 8th week (26.36 ± 4.75%) (Fig. 7E). Group III, after four weeks of treatment, showed severe immunoreactivity (28.79 ± 3.4%) (Fig. 7F), which decreased to mild after the 8th week (16.62 ± 6.48%) (Fig. 7G) (Table 1).

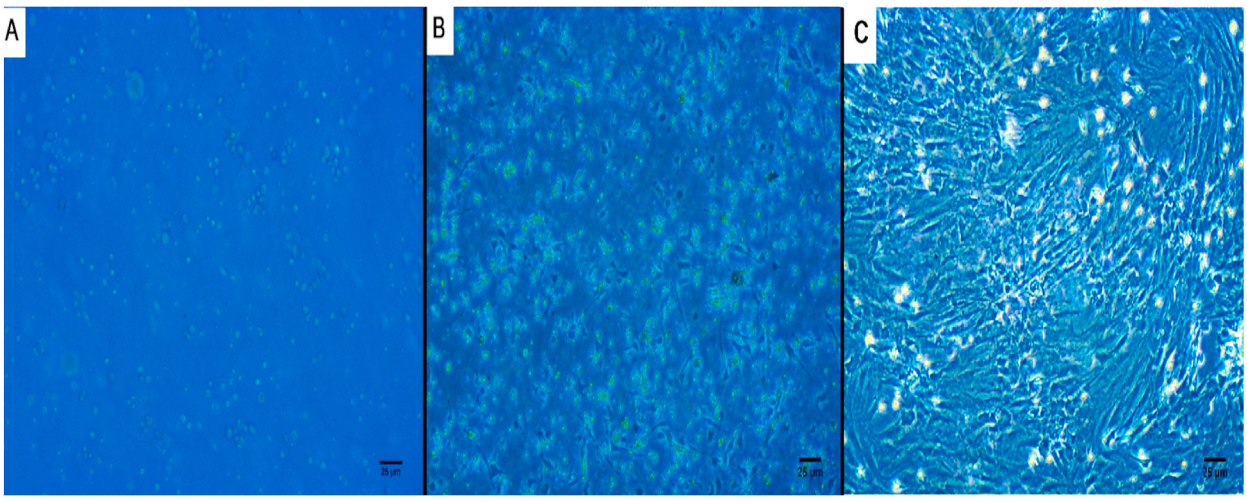

Fig. 3. Inverted microscopy photographs showing a large number of rounded cells on the isolation day (A). Few fibroblast-like cells adhered to the flask at the initial culture on the 3rd day of isolation (B). Cell confluence was noted on the 12th day (C). Scale bar 25 µm.

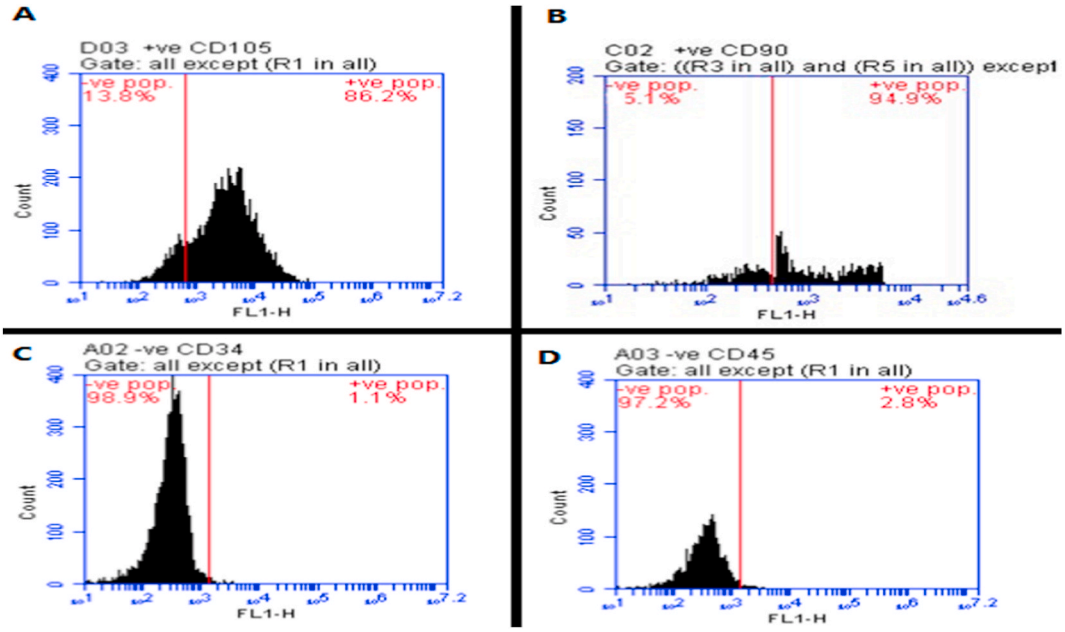

Fig. 4. Flow cytometry chart showing single-parameter histogram for CD105 (A), CD90 (B), CD34 (C), and CD45 (D). Flow cytometric analysis showing the positive reaction for CD105 (86.2%) and CD 90 (94.9%) in BMSCs, while their clusters were negative to CD34 (1.1%), CD 45 (2.8%).

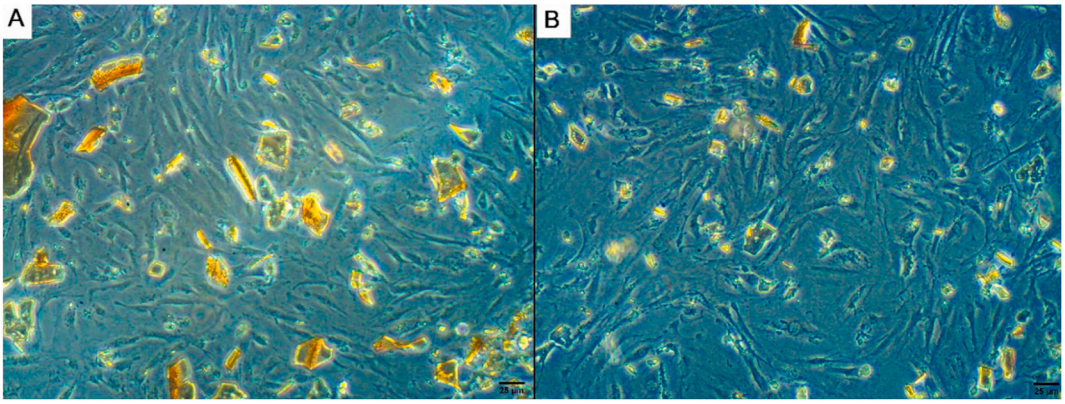

Fig. 5. Inverted microscopy photographs of BMSCs with SPIONs showing SPIONs with in the culture medium before incubation (A) and diffusion of SPIONs within BMSCs after culturing (B). Scale bar 25 μm.

3.4.3. Ultrastructural results

The Electron micrograph of the negative control group revealed normal architecture and arrangement of nerve fibers and Schwan cells, with normal thickness of myelin sheaths around nerve fibers. The endoneurium appeared intact and continuous (Fig. 8A).

The facial nerve trunks in group I, after four weeks of treatment, showed extensive Wallerian degeneration in the form of axonal loss of both large and small fibers with the contortion of myelin sheaths in the form of laminated structures. Very few axons with surrounding Schwann cells were still present, with few marked signs of degeneration (Fig. 8B). After eight weeks of treatment in the same group, the facial nerve trunks showed fibers with increased inter-axonal spaces.

Axons showed signs of degeneration in the form of total axonal loss, shrinkage away from myelin sheaths leaving spaces, and encountering autophagic vacuoles. Myelin sheaths had multiple degeneration profiles such as contortion, thinning, irregular thickening with vacuolation., increased infolding comprising the axons, or formation of redundant outfoldings (Fig. 8C).

The facial nerve trunks showed improved architecture of axons and myelin sheaths in a number of fibers with increased inter-axonal spaces after four weeks of treatment in group II. Fewer fibers showed autophagic vacuoles in axons, in addition to myelin abnormalities in the form of infolding, outfolding, and signs of splitting (Fig. 8D). After eight weeks of the same group, the facial nerve trunks showed nearly normal architecture of axons, Schwann cells and inter-axonal spaces. Signs of degeneration appeared rarely in a few fibers in the form of slight shrinkage of axons and internal separation from myelin sheath, presence of autophagic vacuole, and

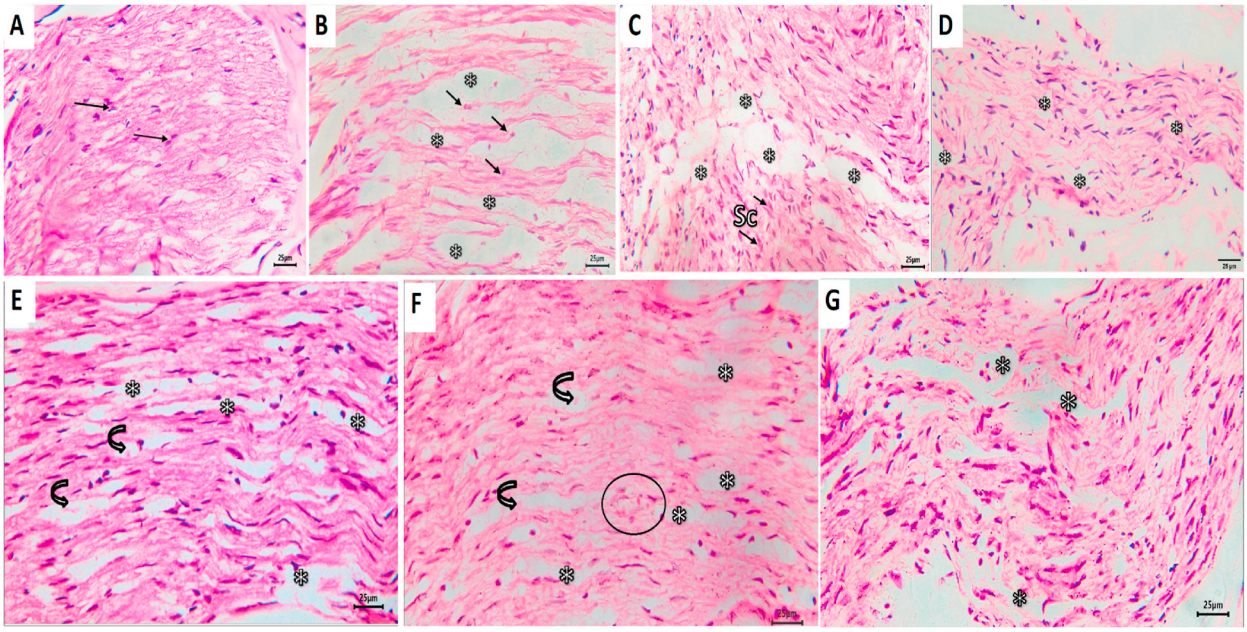

Fig. 6. Photomicrograph of group I showing **A;** normal architecture and arrangement of axons, myelin sheathes and Schwann cells. **B, D & F** represent the results after 4 weeks of treatment for groups I, II, and I, respectively, whereas **C, E &G** represent the results after 8 weeks of treatment for the same groups. Arrows refer to axons' nuclei; asterisks to areas of edema; curved arrows to digestion champers and circle to blood vessel. Sc, Schwann cell, (H&E, scale bar 25 µm).

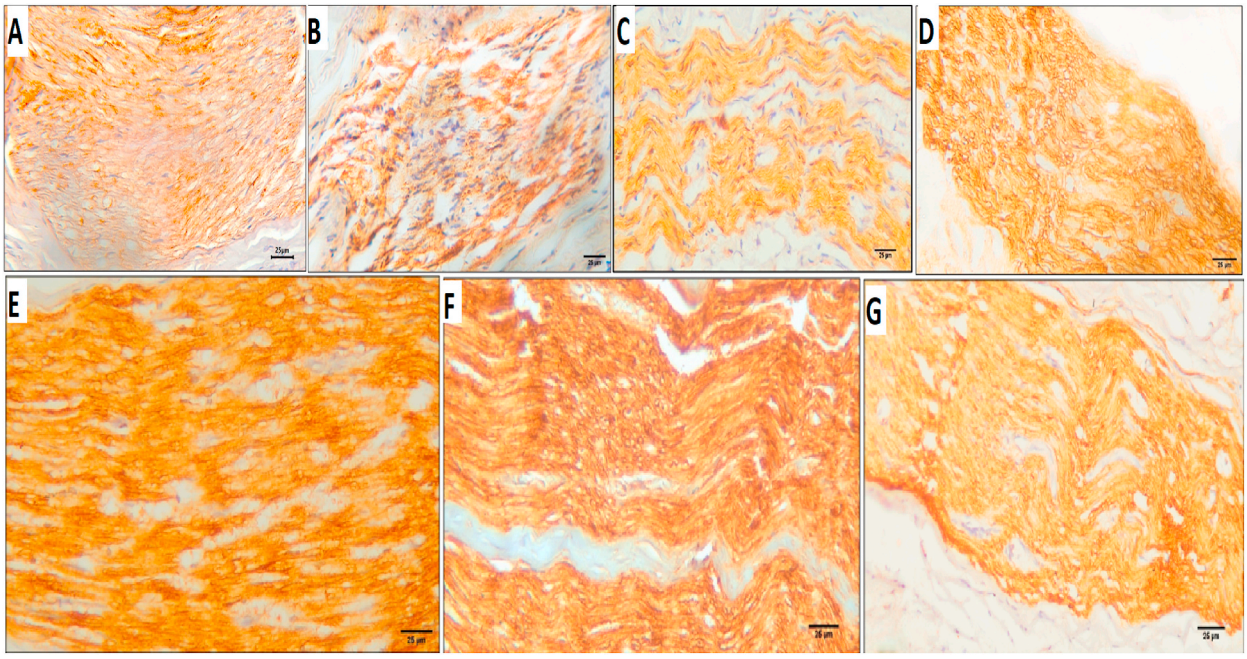

Fig. 7. Anti-S100B-immunostained sections of negative control group showing A; mild level immunoreactivity in myelin sheaths around nerve fibers (16.93 ± 0.06%). B; group I after 4 weeks of treatment showed mild immunoreactivity (18.21 ± 10.17%), C; group I after 8 weeks of treatment showed mild immunoreactivity (13.51 ± 8.05%). D; group II after 4 weeks of treatment showed moderate immunoreactivity (21.99 ± 4.05%), E; immunoreactivity increased to a severe after the 8th week (26.36 ± 4.75%). F; group III after 4 weeks of treatment showed severe immunoreactivity (28.79 ± 3.4%), G; immunoreactivity decreased to a mild after the 8th week (16.62 ± 6.48%) (anti S100; streptavidin-HRP, DAB method, scale bar 25 µm).

Table 1
Comparison between different studied groups according to anti-S100B positively stained mean %Area.

	Negative control		Group I		Group II		Group III		p
	4 weeks (n = 5)	8 weeks (n = 5)	4 weeks (n = 5)	8 weeks (n = 5)	4 weeks (n = 5)	8 weeks (n = 5)	4 weeks (n = 5)	8 weeks (n = 5)	
% Area Mean ± SD.	16.93^{bc} ± 0.06	16.93^{bc} ± 0.06	18.21^{abc} ± 10.17	13.51^{c} ± 8.05	21.99^{abc} ± 4.05	26.36^{ab} ± 4.75	28.79^{a} ± 3.4	16.62^{bc} ± 6.48	**0.002**[a]

p: p value for **F for ANOVA test** for comparing between the studied groups.
Means with **Common letters** are not significant (i.e., Means with **Different letters** are significant).
[a] Statistically significant at $p \leq 0.05$.

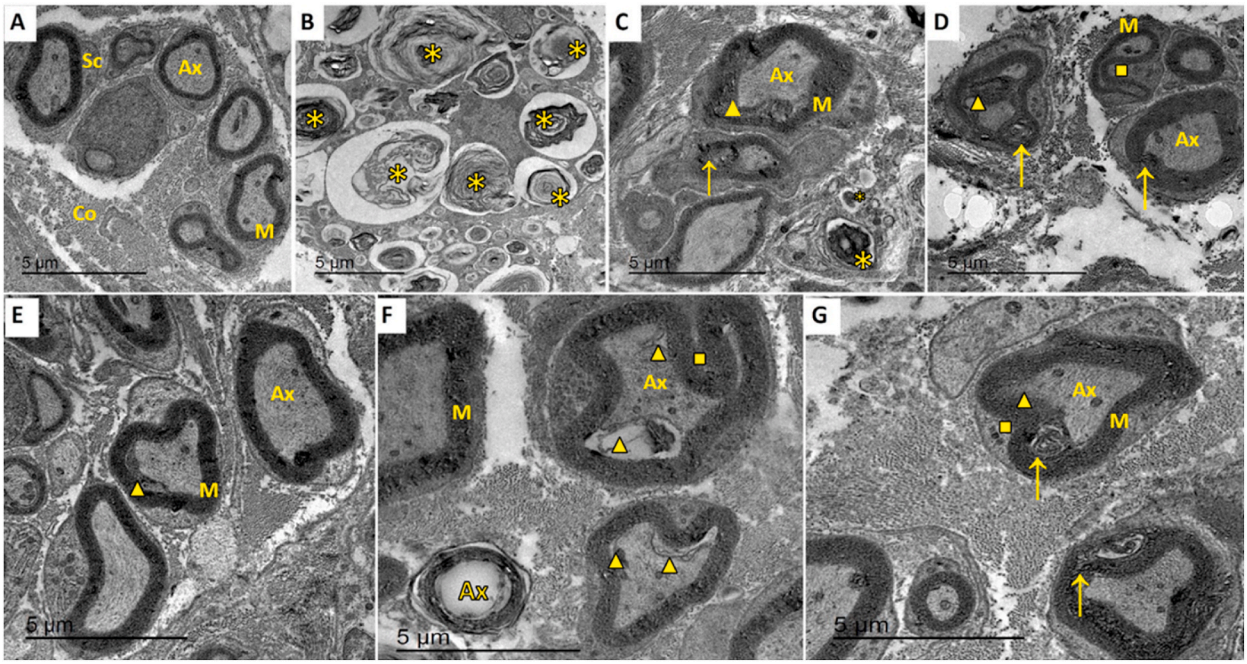

Fig. 8. Transmission electron micrograph of negative control group showing **A;** the normal architecture of nerve fibers. Axons have proper arrangement and thickness of myelin sheaths. **B, D & F** represent the results after 4 weeks of treatment for groups I, II, and I, respectively, whereas **C, E &G** represent the results after 8 weeks of treatment for the same groups. Asterisks refer to areas of axon loss and contortion of myelin sheath, arrows to areas of axon shrinkage away from Schwann cells, triangles to myelin sheath splitting, and squares to myelin sheath infolding. Ax, axon; M, myelin sheath; Sc, Schwann cell; Co, collagen. Scale bar 5 µm.

irregular folding of myelin sheaths (Fig. 8E).

In group III, the facial nerve trunks showed improvement in axons and Schwann cells architecture, with few signs of degeneration in the form of shrinkage of axons away from myelin sheaths and the presence of autophagic vacuole containing degenerated debris after four weeks of treatment. Myelin sheaths showed irregular folding and unfrequented discontinuity (Fig. 8F). However, the facial nerve trunks showed limited improvement in architecture with few signs of degeneration as axon shrinkage, outfolding of myelin sheath with a tendency towards splitting, and the presence of autophagic vacuoles (Fig. 8G).

4. Discussion

Facial nerve regeneration via BMSCs has proved to be a very promising modality for the treatment of facial nerve disorders [18]. Magnetic targeting technology using nanoparticles as SPIO provided an efficient way of stem cell delivery to the exact injured site, increasing the efficacy of stem cell treatment [19,20]. On the other hand, some researchers have raised concerns about the drawbacks of SPION use related to its toxicity towards MSCs and nerve tissue [11].

We hypothesized that BMSC treatment with SPIONs (which act as a stem cell delivery system) might have superior nerve regeneration capacity over that of BMSCs alone. The null hypothesis was that the BMSC-treated group would show similar results to BMSC with SPIONs treated group.

Ethyl alcohol was selected to induce nerve degeneration because it causes nerve blockade that can persist for an extended period, as discussed by **Han et al. (2017)** [21]. Thus, it is already applied as a treatment modality for some peripheral nerve disorders [22].

The histological sections of the negative control group revealed normal architecture and arrangement of Schwan cells, perineurium, and endoneurium, with normal thickness of myelin sheaths around nerve fibers. This was in harmony with **Geuna et al. (2009)**, who investigated the histology of peripheral nerves [23].

Hematoxylin and eosin-stained sections of group I of neurolysed facial trunks after four weeks of treatment were in agreement with those of **Stajčić et al. (1991)** [16]. They found extensive degeneration of infra-orbital nerves in rat models with no signs of regeneration noted four weeks after injection of 90% ethanol. Moreover, **Borin et al. (2006)** hardly noticed any myelinated fibers after three weeks of facial nerve sectioning followed by suturing in Wister rats [24], which agrees with the current results.

The findings of the current study in the same group after eight weeks of treatment were analogous with the findings of **Goel et al. (2009)**, who suggested that regeneration of axons in mammalian peripheral nerves after Wallerian degeneration was limited; however, it was followed by Schwann cells proliferation and activation to compensate the damaged tissue and promote regeneration [25].

Mazoch et al. (2014), contrary to the present results, found that alcohol neurolysis had minimal effect on nerve histology when they studied the impact of alcohol injection, in low doses, into and around rat sciatic nerve. However, this process did not involve the use of alcohol at higher doses [26].

The immunohistochemical findings of anti-S100B staining of this group showed mild immunoreactivity throughout the myelin sheaths around nerve fibers by the end of the 4th week of treatment (18.21% ± 10.17), with minimal change after eight weeks (13.51% ± 8.05). This comes in accordance with **Abbas et al. (2019)**. They noted mild immunoreactivity of anti-S100B in an untreated control group of Wister rats' sciatic nerves after hindlimb amputation followed by re-implantation. They explained these results by the decrease in the number of myelinated fibers as sequelae for degeneration [27].

The ultrastructural results of the same group showed extensive Wallerian degeneration by the end of the 4th week of treatment. After the 8th week of treatment, limited signs of regeneration were seen with increased inter-axonal space. These findings come in harmony with those of **Abbas et al. (2019)**, who detected similar observations in their control untreated groups of sectioned facial nerves [27].

Regarding hematoxylin and eosin-stained sections in this study, the BMSCs-treated group showed a tendency towards regeneration. Better regeneration and arrangement of nerve fibers were observed by the end of the 8th week. These findings agree with the studies conducted by **Goel et al. (2009)**, who studied the impact of bone marrow-derived mononuclear cells on regeneration of transected sciatic nerve in Wister albino rats. They observed a decrease in degeneration signs in histological sections four weeks after treatment, with increased axon regeneration by the end of the 8th week [25].

The present study revealed moderate immunohistochemical reactivity of anti-S100B in the BMSCs-treated group by the end of the 4th week of treatment (21.99% ± 4.05). This immunoreactivity became intense by the end of the 8th week (26.36% ± 4.75). These results coincided with the anti-S100B immunohistochemical results of **Abbas et al. (2019)**, who explained that this high immunoreactivity reflects the increased proliferation of myelinated fibers [27].

The ultrastructural outcomes of the BMSCs-treated group, by the end of the 4th week of treatment, reflected a higher tendency towards regeneration. These results were further improved by the end of the 8th week in the form of nearly normal architecture and arrangement of nerve fibers.

These outcomes align with the ultra-structural findings of **Zarbakhsh et al. (2016)** in the BMSCs-treated groups, which showed regeneration of myelinated axons and proper myelin sheaths. They explained these results by the ability of BMSCs to produce nerve growth factors such as NGF, BDNF, GDNF, CNTF, and NT-3, in addition to substantial extracellular matrix proteins such as collagen I, collagen IV, fibronectin, and laminin [28].

Also, **Wu et al. (2020)**, who studied the co-transplantation of BMSCs and monocytes for the treatment of facial nerve axotomy in Sprague Dawley rats, explained the regenerative impact of BMSCs on the injured nerve by the elevated expression of regulatory cytokines SDF-1 in the injury site. This action upregulates CXCR4 expression in BMSCs, which induces BMSCs to migrate and home in the traumatized nerve region, inhibiting neuronal apoptosis [29]. All the previous data can demonstrate the capacity of BMSCs to orchestrate multiple favorable conditions for facial nerve regeneration, which supports the results of the current study.

Hematoxylin and eosin-stained histological sections of group III, treated with BMSCs and SPIONs, showed regeneration and rearrangement of nerve fibers after four weeks of treatment. The ultra-structural results of the same group in the 4th week of treatment revealed some improvement in axons and Schwann cell architecture.

These results come in harmony with those of **Zhang et al. (2016)**, who indicated that the transplantation of NT3 gene-modified BMSCs conjugated with SPIONs as magnetic carriers could efficiently enhance spinal cord regeneration in rats after 35 days of their experiment. They found that more BMSCs homed the injured site in SPIONs groups, compared with the other groups that did not apply a magnetic targeting technique [10].

Also, the outcomes of **Wu et al. (2020)** agree with the results of the present study after four weeks of treatment. They observed facial nerve regeneration in Sprague Dawley rats in the SPIO-GFP-BMSCs treated groups after 28 days [29].

Unfortunately, the regeneration rate was inversely affected at the end of the 8th week. This was reflected in anti-S100B immunohistochemical results, which decreased to mild reactions (16.62% ± 6.48). Accordingly, the ultra-structural results of the same group showed nearly less improvement in axons and Schwann cells.

Accordingly, the ultra-structural results of the same group showed nearly less improvement in axons and Schwann cells. All these results contradict the hypothesis of **Zhang et al. (2016)** and **Wu et al. (2020)** that the conjugation of SPIONs with BMSCs has superior results in facial nerve regeneration [10,29]. This could be explained by the limited period of both experiments that did not allow examination of the effectiveness of this treatment modality over extended periods.

As a trial to find an explanation for these results, many investigations have studied the biocompatibility of SPIONs with different tissues in general and with the nervous tissues in particular. **Yarjanli et al. (2017)** mentioned that labeling cells with SPIONs for an extended period induces iron accumulation and the production of oxidative stress due to the rise in the amount of reactive oxygen species (ROS). They stated that ROS may directly damage DNA, organelle membranes, and cell membranes [30].

In the same vein, **Imam et al. (2015)** studied the effect of intravenous injection of SPIONs on Sprague Dawley rat brain. They detected the activation of the pro-death compound and c-Abl tyrosine kinase, protein dysfunction in neurons, and expression of α-synuclein, which enhance neuronal damage [31]. These findings agree with the present results after eight weeks of treatment and shed some light on the effectiveness of poly-L-lysine as a coating material in managing the biocompatibility of SPIONs over the long run.

Albukhaty et al. (2013) studied the labeling of neural stem cells with SPIONs for green fluorescent protein transfection in vitro. As in the current study, they used poly-L-lysine as a coating material for SPIONs. They found that poly-L-lysine-coated SPIONs could be used as an effective transfection agent with neural cells [32]. These outcomes were also proved by **Albukhaty et al. (2018)**, who investigated the efficacy of poly-L-lysine-coated SPIONs as a carrier for transferring BDNF into neural stem cells [33].

On the other hand, **Pongrac et al. (2016)** focused on the oxidative stresses of SPIONs with different coating materials on neural stem cells. They compared the effect of uncoated SPIONs, mannose-coated SPIONs, and poly-L-lysine-coated SPIONs. Their results revealed that all of the tested types of SPIONs affected the NSCs by breaking the homeostasis of mitochondria, in addition to disrupting the integrity of CMP and DNA, with no significant differences observed in toxicity endpoints between the different types of coatings used [34].

Singh et al. (2010) explained the generation of ROS by SPIONs despite its coating due to other factors affecting the stability of the coating material itself. These factors include its shelf life and susceptibility to breakdown, whether in vitro or in vivo, which are still not thoroughly investigated [35].

Depending on the outcomes of group III in the current study, it was found that poly-L-lysine-coated SPIONs caused a transient improvement in the regeneration of axons and Schwann cells. This improvement was reversed over a long duration. This could be explained by the susceptible breakdown of poly-L-lysine and the release of ROS induced by uncoated SPIONs, causing cell damage. This explanation needs to be further investigated. Therefore, the assumption of this study was a query since the results of BMSCs alone without SPIONs were better and provided a satisfying improvement of axons and Schwann cells.

5. Conclusion

It could be concluded, within the limitations of this study, that the signs of degeneration within the neurolysed facial nerves have significantly decreased, with the regeneration of axons and myelin sheaths after treatment either with BMSCs only or in conjunction with the magnetic carrier poly-L-lysine coated SPIONs. However, the regeneration degree was diminished compared to that of BMSCs alone over a long duration.

Treatment with neurolysis followed by BMSCs injection may be a promising therapy for the treatment of peripheral nerve disorders such as spasticity, which requires to be investigated in more experimental studies prior to being expressed as an effective way of treatment. Further investigations are needed to study the biocompatibility of SPIONs and their coating materials, used in magnetic targeting or MRI tracking, with stem cells and nervous tissues in the long run.

Ethics approval

All experimental procedures were performed under the protocol approved by the Ethical Committee of the Faculty of Dentistry, Mansoura University, Egypt (Code No. M02260219).

Funding

All authors declare no funding.

Data availability statement

Data is included in the article/supplementary material or referenced in the article.

CRediT authorship contribution statement

Noura Abd El-Latif: Writing – review & editing, Writing – original draft, Methodology, Investigation. **Rehab R. El Zehary:** Writing – review & editing, Supervision, Methodology. **Fatma M. Ibrahim:** Supervision, Project administration, Conceptualization. **Mona Denewar:** Writing – review & editing, Supervision, Methodology.

Declaration of competing interest

The authors declare that they have no known competing financial interests or personal relationships that could have appeared to influence the work reported in this paper.

Acknowledgements

The authors thank Dr/Mohammed Mohsen, Lecturer of Radiology, Faculty of Medicine, Mansoura University, for his assistance in the radiographic procedures in the research.

Appendix A. Supplementary data

Supplementary data to this article can be found online at https://doi.org/10.1016/j.heliyon.2024.e26675.

References

[1] C.R. Spencer, R.M. Irving, Causes and management of facial nerve palsy, Br. J. Hosp. Med. 77 (2016) 686–691, https://doi.org/10.12968/hmed.2016.77.12.686.
[2] A. Calodney, R. Rosenthal, A. Gordon, R.E. Wright, Targeted Radiofrequency Techniques , Techniques of Neurolysis, Springer, 2016, https://doi.org/10.1007/978-3-319-27607-6_3.
[3] M.M. Hanania, C.E. Argoff, Permanent Neural Blockade and Chemical Ablation, Pain Management Secrets, third ed. ed, Elsevier, 2009 eBook 978-0-323-41386-2.
[4] T.I. Mitrano, M.S. Grob, F. Carrion, E. Nova-Lamperti, P.A. Luz, F.S. Fierro, et al., Culture and characterization of mesenchymal stem cells from human gingival tissue, J. Periodontol. 81 (2010) 917–925, https://doi.org/10.1902/jop.2010.090566.
[5] I. Ullah, R.B. Subbarao, G.J. Rho, Human mesenchymal stem cells-current trends and future prospective, Biosci. Rep. 35 (2015), https://doi.org/10.1042/BSR20150025.
[6] Y. Matsuda, M. Sasaki, Y. Kataoka-Sasaki, A. Takayanagi, K. Kobayashi, S. Oka, et al., Intravenous infusion of bone marrow–derived mesenchymal stem cells reduces erectile dysfunction following cavernous nerve injury in rats, Sex. Med. 6 (2018) 49–57, https://doi.org/10.1016/j.esxm.2017.10.005.
[7] S. Nemati Mahand, N. Niknami, A. Moghaddam, S. Nemati Mahand, A. Salehi Moghaddam, M. Arjmand, et al., Application of stem cells, growth factors, small molecules, and biological macromolecules on nerve regeneration: a review and future direction, Int. J. Polym. Mater. 30 (2023) 1–33, https://doi.org/10.1080/00914037.2023.2215376.
[8] Z. Khodabandeh, D. Mehrabani, F. Dehghani, N. Gashmardi, M. Erfanizadeh, S. Zare, F. Bozorg-Ghalati, Spinal cord injury repair using mesenchymal stem cells derived from bone marrow in mice: a stereological study, Acta Histochem. 123 (5) (2021) 151720, https://doi.org/10.1016/j.acthis.2021.151720.
[9] N. Landázuri, S. Tong, J. Suo, G. Joseph, D. Weiss, D.J. Sutcliffe, et al., Magnetic targeting of human mesenchymal stem cells with internalized superparamagnetic iron oxide nanoparticles, Small 9 (2013) 4017–4026, https://doi.org/10.1002/smll.201300570.
[10] R.P. Zhang, L.J. Wang, S. He, J. Xie, J.D. Li, Effects of magnetically guided, SPIO-labeled, and neurotrophin-3 gene-modified bone mesenchymal stem cells in a rat model of spinal cord injury, Stem Cell. Int. (2016), https://doi.org/10.1155/2016/2018474.
[11] A. Nemmar, S. Beegam, P. Yuvaraju, J. Yasin, S. Tariq, S. Attoub, et al., Ultrasmall superparamagnetic iron oxide nanoparticles acutely promote thrombosis and cardiac oxidative stress and DNA damage in mice, Part. Fibre Toxicol. 13 (2015) 1–11, https://doi.org/10.1186/s12989-016-0132-x.
[12] M. Mahdavi, M.B. Ahmad, M.J. Haron, F. Namvar, B. Nadi, M.Z.A. Rahman, et al., Synthesis, surface modification and characterisation of biocompatible magnetic iron oxide nanoparticles for biomedical applications, Molecules 18 (2013) 7533–7548, https://doi.org/10.3390/molecules18077533.
[13] D. Mehrabani, M. Nazempour, R. Mehdinavaz-Aghdam, S.S. Hashemi, R. Jalli, M.S. Moghadam, et al., MRI tracking of human Wharton's jelly stem cells seeded onto acellular dermal matrix labeled with superparamagnetic iron oxide nanoparticles in burn wounds, Burns & Trauma 10 (2022), https://doi.org/10.1093/burnst/tkac018 tkac018.
[14] R.M. Patil, N.D. Thorat, P.B. Shete, P.A. Bedge, S. Gavde, M.G. Joshi, et al., Comprehensive cytotoxicity studies of superparamagnetic iron oxide nanoparticles, Biochem Biophys Rep 13 (2018) 63–72, https://doi.org/10.1016/j.bbrep.2017.12.002.
[15] R. Jalli, D. Mehrabani, S. Zare, M. Saeedi Moghadam, I. Jamhiri, N. Manafi, et al., Cell proliferation, viability, differentiation, and apoptosis of iron oxide labeled stem cells transfected with lipofectamine assessed by MRI, J. Clin. Med. 12 (6) (2023) 2395, https://doi.org/10.3390/jcm12062395.
[16] Z. Stajčić, Effects of glycerol on the rat infraorbital nerve: an experimental study, Br. J. Oral Maxillofac. Surg. 29 (1991) 90–93, https://doi.org/10.1016/0266-4356(91)90088-M.
[17] T. Hadlock, J. Kowaleski, R.Lo D. Bermejo, H.P. Zeigler, S. Mackinnon, et al., Functional assessments of the rodent facial nerve: a synkinesis model, Laryngoscope 118 (2008) 1744–1749, https://doi.org/10.1097/MLG.0b013e31817f5255.
[18] S. Huang, L. Xu, Y. Sun, T. Wu, K. Wang, G. Li, An improved protocol for isolation and culture of mesenchymal stem cells from mouse bone marrow, JOT 3 (2015) 26–33, https://doi.org/10.1016/j.jot.2014.07.005.
[19] L.H. Silva, F.F. Cruz, M.M. Morales, D.J. Weiss, P.R. Rocco, Magnetic targeting as a strategy to enhance therapeutic effects of mesenchymal stromal cells, Stem Cell. Res. J. 8 (2017) 1–8, https://doi.org/10.1186/s13287-017-0523-4.
[20] E. Taboada, E. Rodríguez, A. Roig, J. Oró, A. Roch, R.N. Muller, Relaxometric and magnetic characterization of ultrasmall iron oxide nanoparticles with high magnetization. Evaluation as potential T 1 magnetic resonance imaging contrast agents for molecular imaging, Langmuir 23 (2007) 4583–4588, https://doi.org/10.1021/la063415s.
[21] K.R. Han, Y.J. Chae, J.D. Lee, C. Kim, Trigeminal nerve block with alcohol for medically intractable classic trigeminal neuralgia: long-term clinical effectiveness on pain, Int. J. Med. Sci. 14 (2017) 29, https://doi.org/10.7150/ijms.16964.
[22] R. Wu, B.S. Majdalany, M. Lilly, J.D. Prologo Jd, N. Kokabi, Agents used for nerve blocks and neurolysis, InSeminars in Interventional Radiology 39 (No. 04) (2022 Aug) 387–393, 333 Seventh Avenue, 18th Floor, New York, NY 10001, USA: Thieme Medical Publishers, Inc.
[23] S. Geuna, S. Raimondo, G. Ronchi, F. Di Scipio, P. Tos, K. Czaja, et al., Histology of the peripheral nerve and changes occurring during nerve regeneration, Int. Rev. Neurobiol. 87 (2009) 27–46, https://doi.org/10.1016/S0074-7742(09)87003-7.
[24] A. Borin, R.N. Toledo, S.D. de Faria, J.R.G. Testa, O.L.M. Cruz, Behavioral and histologic experimental model of facial nerve regeneration in rats, Braz J Otorhinolaryngol 72 (2006) 776–785, https://doi.org/10.1016/S1808-8694(15)31044-2.
[25] R.K. Goel, V. Suri, A. Suri, C. Sarkar, S. Mohanty, M.C. Sharma, et al., Effect of bone marrow-derived mononuclear cells on nerve regeneration in the transection model of the rat sciatic nerve, J. Clin. Neurosci. 16 (2009) 1211–1217, https://doi.org/10.1016/j.jocn.2009.01.031.
[26] M.J. Mazoch, G.A. Cheema, L.J. Suva, R.L. Thomas, Effects of alcohol injection in rat sciatic nerve as a model for Morton's neuroma treatment, Foot Ankle Int. 35 (2014) 1187–1191, https://doi.org/10.1177/1071100714546188.
[27] O.L. Abbas, O. Özatik, Z.B. Gönen, A.E. Koçman, I. Dag, F.Y. Özatik, et al., Bone marrow mesenchymal stem cell transplantation enhances nerve regeneration in a rat model of hindlimb replantation, Plast Reconst Surg 143 (2019) 758e, https://doi.org/10.1097/PRS.0000000000005412, 68e.
[28] S. Zarbakhsh, N. Goudarzi, M. Shirmohammadi, M. Safari, Histological study of bone marrow and umbilical cord stromal cell transplantation in regenerating rat peripheral nerve, Cell J 17 (2016) 668, https://doi.org/10.22074/cellj.2016.3839.
[29] L. Wu, D. Han, J. Jiang, X. Xie, X. Zhao, T. Ke, et al., Co-transplantation of bone marrow mesenchymal stem cells and monocytes in the brain stem to repair the facial nerve axotomy, EJH 64 (2020), https://doi.org/10.4081/ejh.2020.3136.

[30] Z. Yarjanli, K. Ghaedi, A. Esmaeili, S. Rahgozar, A.J.B. Zarrabi, Iron oxide nanoparticles may damage to the neural tissue through iron accumulation, oxidative stress, and protein aggregation, BMC Neurosci. 18 (2017) 1–12, https://doi.org/10.1186/s12868-017-0369-9.
[31] S.Z. Imam, S.M. Lantz-McPeak, E. Cuevas, H. Rosas-Hernandez, S. Liachenko, Y. Zhang, et al., Iron oxide nanoparticles induce dopaminergic damage: in vitro pathways and in vivo imaging reveals mechanism of neuronal damage, Mol. Neurobiol. 52 (2015) 913–926, https://doi.org/10.1007/s12035-015-9259-2.
[32] S. Albukhaty, H. Naderi-Manesh, T. Tiraihi, In vitro labeling of neural stem cells with poly-L-lysine coated super paramagnetic nanoparticles for green fluorescent protein transfection, Iran. Biomed. J. 17 (2) (2013) 71, https://doi.org/10.6091/ibj.1114.2013.
[33] S. Albukhaty, H. Naderi-Manesh, T. Tiraihi, M. Sakhi Jabir, Poly-l-lysine-coated superparamagnetic nanoparticles: a novel method for the transfection of pro-BDNF into neural stem cells, Artif. Cells, Nanomed. Biotechnol. 46 (2018) S125–S132, https://doi.org/10.1080/21691401.2018.1489272.
[34] I.M. Pongrac, I. Pavičić, M. Milić, L.B. Ahmed, M. Babič, D. Horák, et al., Oxidative stress response in neural stem cells exposed to different superparamagnetic iron oxide nanoparticles, Int J Nanomedicine 11 (2016) 1701, https://doi.org/10.2147/IJN.S102730.
[35] N. Singh, G.J. Jenkins, R. Asadi, S.H. Doak, Potential toxicity of superparamagnetic iron oxide nanoparticles (SPION), Nano Rev. 1 (1) (2010) 5358, https://doi.org/10.3402/nano.v1i0.5358.